CERN/LHCC 97-39
Status Report/RD48
20 June 1997

RD48 STATUS REPORT

The ROSE Collaboration
(R&d On Silicon for future Experiments)

Co-Spokespersons: Francois Lemeilleur, Gunnar Lindstroem, Steve Watts

Bari University, Italy
V. Augelli, M. Angarano, D. Creanza, M. De Palma, L. Schiavulli

Berkeley, University of California, Dept. of Materials Science, USA
E. Weber

Brookhaven National Laboratory, USA.
Z. Li, H.W. Kraner

Bucharest, Institute of Nuclear Physics and Engineering, Romania
A. Vasilescu

Bucharest, Institute of Physics and Technology of Materials, Romania
T. Botila, D. Petre, I. Pintilie, L. Pintilie

Catania University, Italy
S. Albergo, D. Boemi, R. Potenza, A. Tricomi

CERN, Switzerland
F. Lemeilleur, G. Casse, B. Dezillie, M. Glaser, C. Leroy, P. Riedler,
S. Roe, P. Weilhammer, K. Zankel

Demokritos, Institute of Nuclear Physics, Greece
G. Fanourakis, D. Loukas, A. Markou, I. Siotis, S. Tzamarias, A. Vayaki

Dortmund University, Germany
R. Wunstorf, C. Becker

Fermilab, Batavia (IL), USA
S. Kwan, D. Anderson

Firenze University, Italy
M.Bruzzi, U. Biggeri, E.Borchi, E.Catacchini, E. Focardi, G. Parrini

Gent University, Belgium
P. Clauws

Glasgow University, U.K.
K. Smith, R. Bates, C. Da Viai, S. Manolopoulos, V. Oshea, A. Pickford, C. Raine

Hamburg University, Germany
G. Lindstroem, H. Feick, E. Fretwurst, M. Moll

Karlsruhe University
W. de Boer, D. Knoblauch, S. Meyer

Kiev, Institute for Nuclear Research, Academy of Sciences, Ukraine
P. Litovchenko

Lancaster University, UK
T. Sloan, L. Beatty, T. Brodbeck, A. Chilingarov, G. Hughes, P. Ratoff, B.K.Jones,
S. McGarry, M.Mcpherson

Liverpool University, U.K.
P. Allport, M. Hanlon

London, Brunel University, UK
S. Watts, A. Holmes-Siedle, J. Matheson, M. Ahmed, M. Solanky

London, Imperial College, UK.
G. Hall, B. MacEvoy

London, Kings College, UK
G. Davies

Lubiana, J. Stephan Institute, Slovenia
M. Mikuz

Minsk, Institute of Applied physics, Bielorussia
P. Kuchinski

Modena University, Italy
G. Ottaviani

Munich, Max Planck Institute, Germany
G. Lutz, R.H. Richter

Padova University, Italy
D. Bisello, N. Bacchetta, A. Giraldo

Perugia University, Italy
G.M. Bilei, P. Bartalini, P. Ciampolini, D. Passeri, A. Santocchia

Pisa, INFN, Italy.
G. Tonelli, R. Dell'Orso, A. Messineo, P. Verdini, R. Wheadon

Prague, Nuclear Center of Charles University
I. Wilhelm

Prague, Czech Technical University, Czech Republic
B. Sopko, S. Pospisil

Prague, Institute of Physics, Academy of Sciences, Czech Republic
V. Vrba, P. Sicho

Stockholm, Royal Institute of Technology, Sweden
B. Swenson

St Petersburg, Ioffe Physico-Technical Institute, Russia
E. Verbitskaya, V. Eremin

Villigen, PSI, Switzerland
K. Gabathuler, R. Horisberger

Warsaw, Institute of Electronic Materials Technology (ITME), Poland
Z. Luczynski, E. Nossarzewska, P. Zabierowski

Associated Companies:

Canberra Semiconductor, Belgium
P. Burger

Micron Semiconductor, U.K.
C. Wilburn

SINTEF, Norway
L.Evensen

Observers:

European Space Agency, ESTEC, Solar System Division, Holland
B. Johlander

IMEC, Belgium
C. Claeys, E. Simoen

LEPES, Grenoble, France
J-C. Bruyere

Max Planck Institute, Munich, Germany
J. Kemmer, N. Meidinger

1. Introduction

This is the first status report of the RD48 or ROSE Collaboration. The Collaboration is concentrating on the problems of bulk damage in silicon resulting from irradiation by hadrons. The main scientific results are outlined. For detailed information, references are made to the relevant paper, technical note or workshop talk. More results are expected in the coming year. However, preliminary recommendations are made concerning the choice of material for silicon trackers that are used in harsh radiation environments.

1.1. The ROSE Collaboration - Overview

The ROSE Collaboration consists of international groups working on detectors for particle physics experiments at the LHC. In addition, the Collaboration benefits from the very valuable input of solid state physicists and the expertise of silicon manufacturers. The Collaboration formed following the First Workshop on Radiation Hardening of Silicon Detectors, at CERN in October 1995. The proposal [1] was approved by the LHCC in June 1996. The Second Workshop was held at CERN in February 1997 - see Appendix 1. There were about 100 participants from 30 groups and 40 talks were given. Copies of transparencies from these workshops are available [2]. A World-Wide-Web page also provides useful information [3].

Lancaster, Liverpool, Glasgow, Royal Institute of Technology, Stockholm, Karlsruhe, Aarhus and ITME joined the collaboration at the February collboration meeting. The close involvement of Canberra, Micron and SINTEF is shown through their "Associated Company" status. It is proposed to hold the 3rd Workshop at DESY in late September 1997.

The objectives of the collaboration are,

a) To develop radiation hard detectors that can operate beyond the limits of present devices and that ensure guaranteed operation for the whole lifetime of the LHC experimental programme.

b) To make recommendations to experiments on the optimum silicon for detectors and quality control procedures required to ensure optimal radiation tolerance.

The key idea is that one can improve the radiation tolerance of silicon by defect engineering. Defect engineering involves the deliberate addition of impurities to silicon in order to effect the formation of electrically active defect centres and thus control the macroscopic parameters of devices. Key ingredients to investigate are oxygen and carbon because they act as sinks for vacancies and interstitials. But other more exotic impurities are also being studied. The defect engineering strategy is illustrated in figure 1.1. One must obtain material with differing impurity levels, characterise the material, irradiate, then measure defect concentrations and macroscopic parameters. Macroscopic changes are then understood using defect kinetics and device models.

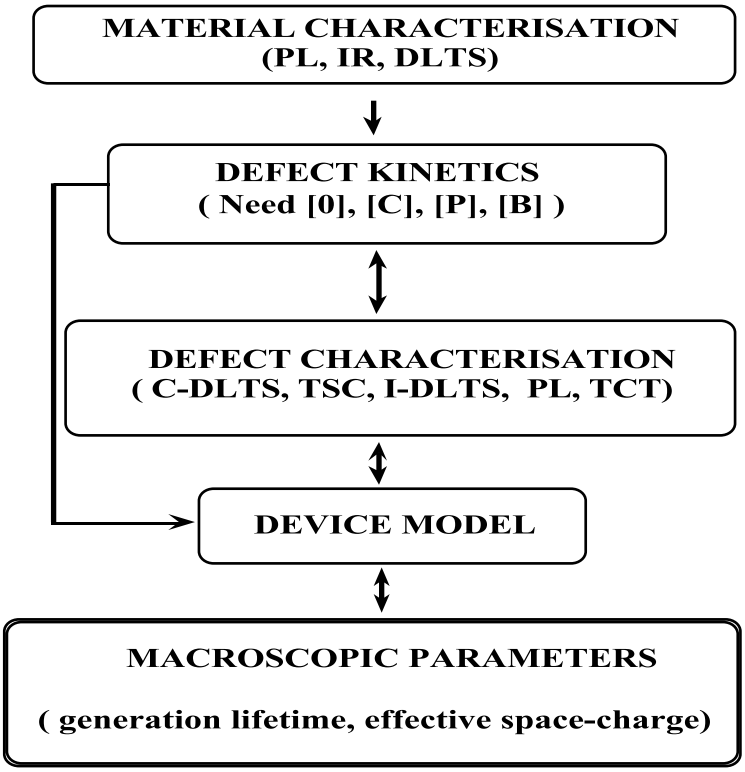

Figure 1.1 Defect Engineering Strategy

The current status of the work is summarised in Table 1.1. Testing is in three categories; material characterisation, defect characterisation and macroscopic characterisation after irradiation (IV, CV etc.). "☆" means "In progress" . ✔ means "Finished", ✗ means " To be done" .

Material	Manufacturer	Made	Tested See above
Standard FZ	Wacker + others	✔	✔✔✔
Epitaxial	MACOM	✔	✔☆✔
Epitaxial	ITME	✔	✔✗✔
Fz + O OFZ/G	Polovodice	✔	✔☆✔
Fz + C	Polovodice	Due end June	✗ ✗ ✗
Fz + N	Polovodice	✔	☆ ✗ ✔
Fz + O + C	Polovodice	Ordered	✗ ✗ ✗
Fz + 0.1% Ge	Topsil	✔	☆☆✔
Fz + Sn	Topsil/Aarhus	✔	✗ ☆☆
Fz + Sn	Polovodice	Ordered	✗ ✗ ✗
Fz + O OFZ/Q	ITME	Ordered	✗ ✗ ✗
CZ 100 ohm.cm	Polovodice	✔	✔ ✗ ✔

Table 1.1 Status of materials under investigation by the ROSE Collaboration.

Material and diodes have been distributed widely throughout the Collaboration - Appendix 2.

The range of oxygen and carbon concentrations covered by the various materials is indicated in Figure 1.2. Infra-red absorption has been used to obtain these concentrations in float zone material. Epitaxial layers have been studied using Secondary Ion Mass Spectroscopy (SIMS). Although SIMS cannot detect very low concentrations, it has proven invaluable to this project. A commercial company (Charles Evans and Associates), has been able to do the work quickly with excellent detection limits. This has proven to be an expensive technique but well worthwhile in terms of the information it has given. Photoluminescence has proven to be the best technique for checking the phosphorus/boron compensation.

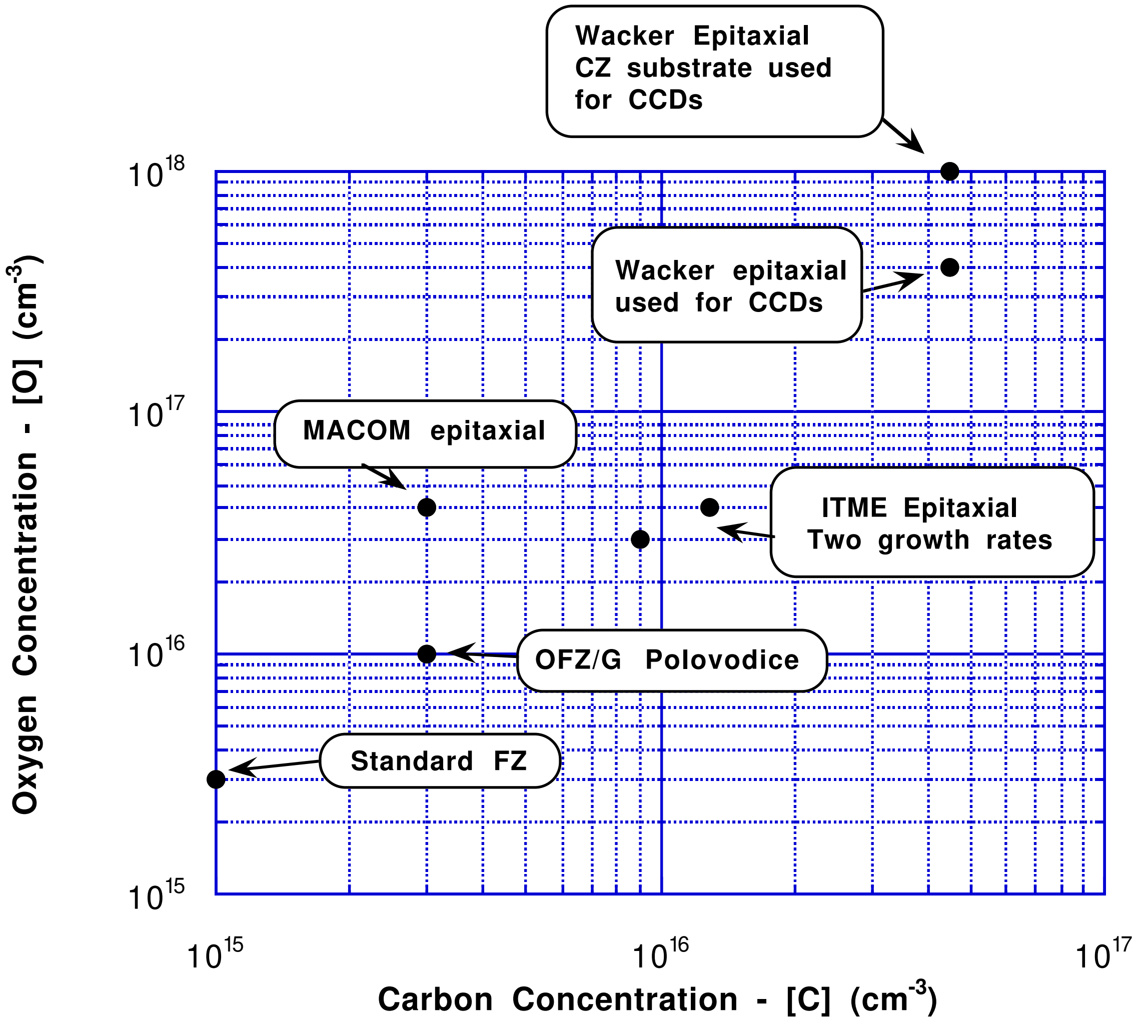

Figure 1.2 Oxygen and carbon concentrations in the various material obtained by the ROSE Collaboration. The two growth rates for ITME epitaxial were 0.5 and 1.0 micron/min. The slower growth rate has the higher carbon concentration.

2. Summary of key new results

This section provides an executive summary. More details can be found in later sections and references therein.

- The charge collection efficiency for standard material has been measured up to fluences of 10^{15} n cm^{-2}. Typically 40% of the charge remains after such a fluence. See Section 3.1.

- Reverse annealing data is described well with a second-order parameterisation. However, new results show that the rate constant is inversely proportional to the fluence. This means that a first-order dissassociation or re-ordering process is responsible. Damage projections for the trackers may need recalculating. See Sections 3.2 and 7 for further comments.

- Measurements of the conductivity of silicon as a function of temperature before and after irradiation clearly confirm that the material in equilibrium (no external bias) is close to intrinsic after irradiation. See Section 3.3.

- Epitaxial material (n and p-type) has been grown up to thicknesses of 200 microns by ITME in Poland. N-type material obtained by Canberra from Macom in the USA shows a factor 2 improvement in its inversion fluence compared to float-zone. Material grown by ITME degrades in a similar way to float-zone when irradiated. The main difference between the two sources is the carbon concentration which is a factor three higher in the ITME material. First results on p-type epitaxial are also to be found in this report. Epitaxial material looks promising for pixel detectors although further work is required. See Section 3.4.

- Oxygenated float zone manufactured using gas doping (OFZ/G) can achieve a maximum oxygen concentration of around 10^{16} cm^{-3}. No significant differences are found between this material and standard float zone. However, a different process developed by Wacker using a quartz ring on the float-zone (OFZ/Q) can achieve high oxygen concentrations. An order has been placed to manufacture some of this material. From work on epitaxial wafers, we expect OFZ/Q material to be a factor two better than standard float zone. See Section 3.5 for further information.

- Nitrogenated float zone manufactured using gas doping (NFZ/G) has been produced but degrades in a similar to standard float zone. Work is in progress to confirm the nitrogen levels in the material.

- Two defect signals have been correlated with reverse annealing; a bistable acceptor in the bottom half of the bandgap (E_V +0.32 eV), and the photoluminescence W-line. This is the first time that this macroscopic behaviour has been correlated with a microscopic signal. The appearance of the W-line indicates that an intrinsic, interstitial related defect is linked to this behaviour. This implies that it will be difficult to "defect engineer" this behaviour. However, some differences are seen with CZ material. See Section 4.

- The annealing behaviour of the leakage current and effective doping concentration has been correlated with intrinsic defects - probably multi-vacancy - associated with damage clusters. See Section 4.

● There is now substantial evidence for Inter-Centre Charge Transfer of electrons between defects inside terminal clusters. This enhances the occupancy of these levels by a factor 100 or more and leads to larger leakage current than would be expected on the basis of defect concentrations and standard Shockley-Read-Hall statistics. See Section 4.

● There are indications that the "hardness factor" for 24 GeV/c protons is a factor two less than had been thought. This is actively being studied. Section 5 provides recommendations for silicon displacement damage functions to be used by experiments.

● We have few diodes made on p-type high resistivity tin doped float zone material. This material is expected to be the most radiation tolerant. Results are expected in the near future.

3. Macroscopic Data

This section describes some of the latest measurements on macroscopic parameters - IV, CV, charge collection. These parameters decide whether the detector is useable. For completeness, a short summary of bulk damage effects is given in this introduction and then new results are discussed.

Detector leakage currents increase significantly during irradiation. The current is described in terms of J_v, which is the leakage current per unit volume. It is well established that the increase in J_v is directly proportional to particle fluence:

$$\Delta J_v = \alpha \Phi \tag{1}$$

The proportionality constant, α, is known as the "damage" constant and has the value (5-10)$\times 10^{-17}$ A.cm^{-1} immediately after irradiation [4]. An exp($-E_g/2kT$) temperature dependence can be used. The leakage current is observed to anneal exponentially after the end of irradiation with a series of time constants, all of which are temperature dependent. At room temperature the current anneals by ~50% over a period of about 14 days.

In an unirradiated device, the space-charge results from shallow dopants in the silicon, usually phosphorus and boron. Photoluminescence studies of n-type silicon indicate that the level of compensation by boron contamination is very low. Irradiation results in an accumulation of negative space-charge in the depletion region due to the introduction of deep levels. N-type detectors therefore become progressively less n-type with increasing hadron fluence until they invert to effectively p-type at around 2×10^{13} n.cm^{-2} and then continue to become more p-type beyond this point, apparently without limit [5,6]. Typical results are shown in Fig. 3.1. In practice, the detectors still work beyond the inversion fluence because the junction moves from the p^+ strips to the n^+ back-plane contact. The effective doping concentration, N_{eff}, can be inferred from the voltage required to obtain full depletion, V_{depl}:

$$N_{eff} = \frac{2\varepsilon_0 \varepsilon_{Si}}{ed^2} V_{depl} \tag{2}$$

where d is the diode thickness. At high fluences, N_{eff} can be such that the depletion voltage exceeds the breakdown voltage of the device and efficient operation is no longer possible. This effect represents the limiting factor for long-term operation at the LHC.

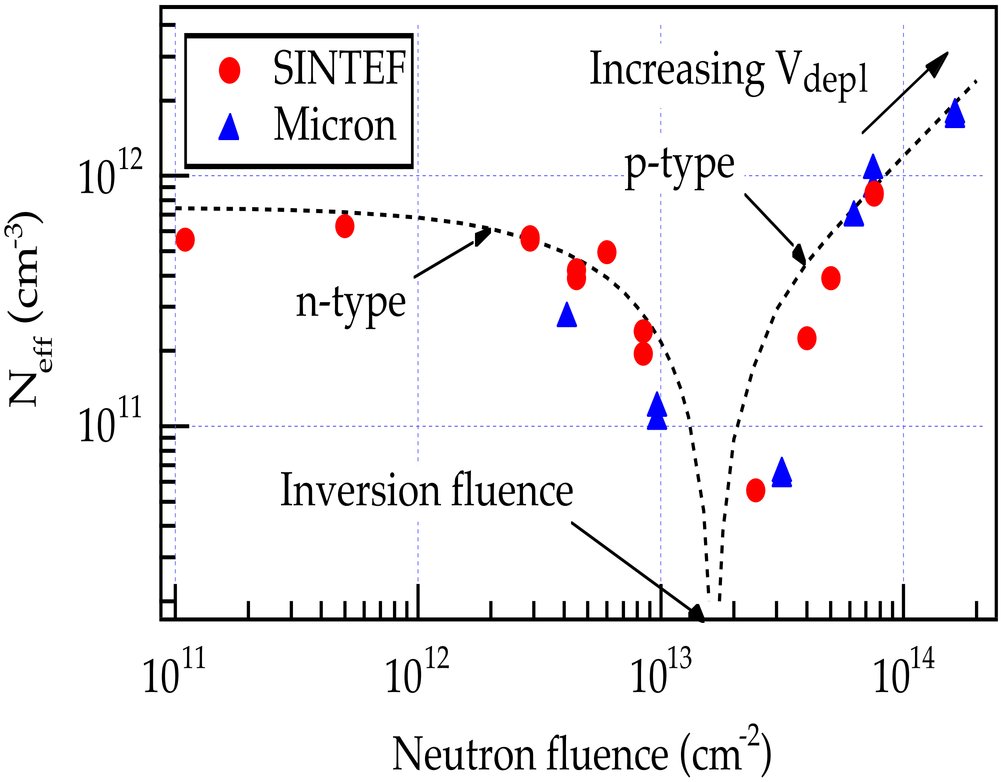

Fig. 3.1. Evolution of N_{eff} with neutron fluence for high resistivity n-type detectors from two manufacturers on standard float zone.

In the period after irradiation, the annealing behaviour of N_{eff} displays two distinct phases. There is an initial reduction in negative space-charge, which is later dominated by a slower, but much larger, increase in acceptor concentration. This second phase is known as "reverse annealing". The rate at which reverse annealing proceeds is highly temperature dependent; the changes can take tens of years at 0˚C but are accelerated to a matter of hours at 100˚C.

On account of the leakage current and reverse annealing, detectors at the LHC will have to be operated below room temperature. Warm up/maintenance periods need to be included in detector damage projections as they can have a major influence on these calculations.

3.1 Charge Collection Efficiency

Until the February Workshop, there were no measurements beyond 10^{14} n cm^{-2} where a 10% loss was seen. New results were presented by Lancaster (1 MeV ISIS neutrons), PSI (300 MeV/c pions) and Marseille (300 MeV protons). The data from Lancaster and Marseille is plotted together in Fig. 3.2. Indications are that 40% of the signal will remain after 10^{15} 1 MeV equivalent n cm^{-2}.

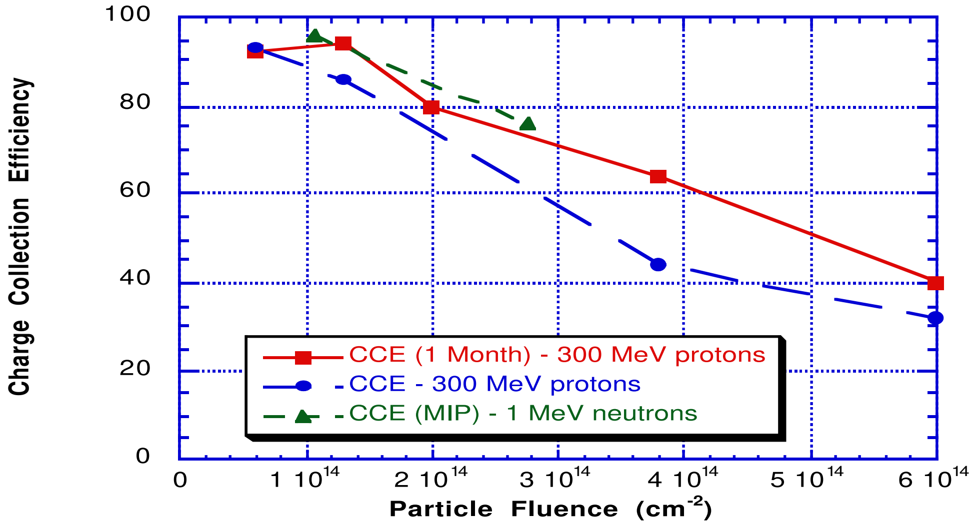

Fig 3.2 Charge collection measurements from February ROSE Workshop. Data from Lancaster and Marseille. 300 MeV protons have a NIEL which is a factor 1.7 higher than 1 MeV neutrons.The proton data shows some recovery after 1 month.

3.2 Reverse Annealing

Reverse annealing data is fitted best with a second-order parameterisation. Fig 3.3 from reference [7] shows that the rate constant is inversely proportional to the fluence. This means that a first-order dissassociation or re-ordering process is responsible.

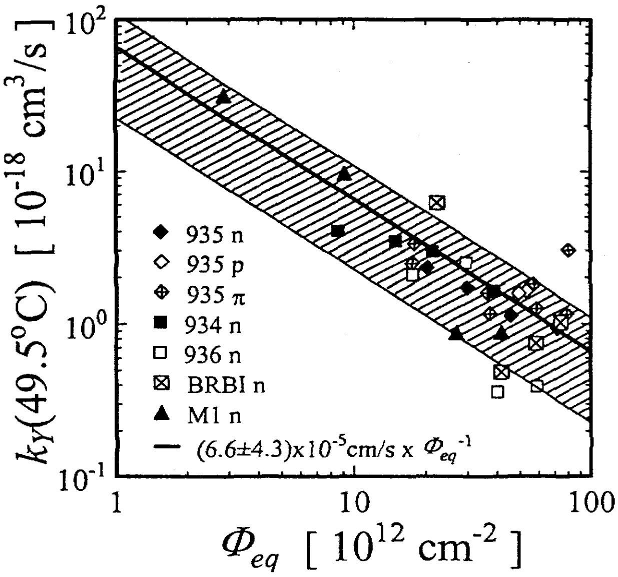

Fig 3.3 Reverse annealing rate constant at 49.5 ^oC as a function of fluence for various wafers and particle types. From ref. [7].

The rate constant dependence on fluence, ϕ , can be parametrised as,

$$k_y(\phi) = k_o(\phi)\exp(-1.31eV/kT) \text{ with } k_o = (1.9 +/-1.2)\, 10^{16}\ cm/s\ .\ \phi^{-1} \qquad (3)$$

Ref. [7] should be consulted for more details. This result means that damage projections for the LHC trackers should be recalculated. Typically, 20 °C rate constants of about $1.5\ 10^{-20}\ cm^3\ s^{-1}$ are used. This corresponds to a fluence of a few $10^{13}\ n\ cm^{-2}$. A new damage projection analysis is given in Section 7 and shows the effect of this revision to the model.

3.3 Behaviour of the irradiated silicon in equilibrium

It has been known for many years that the Fermi level of heavily irradiated silicon is close to mid-gap, i.e. that the material in equilibrium looks like an intrinsic semiconductor. Recent measurements of the conductivity of irradiated and non-irradiated samples as a function of temperature clearly shows this fact, ref. [8]. The conductivity of the irradiated samples drops dramatically with temperature. The activation energy is around 0.53 eV. Refs. [7] and [9] show that these results are in good agreement with the calculation of the Fermi level position based on defect concentrations determined by deep level spectroscopy. Phosphorus removal is not required, and recent studies, [7], have confirmed earlier measurements, [10], that the production of vacancy-phosphorus centres in standard material is suppressed due to the large [O]/[P] ratio.

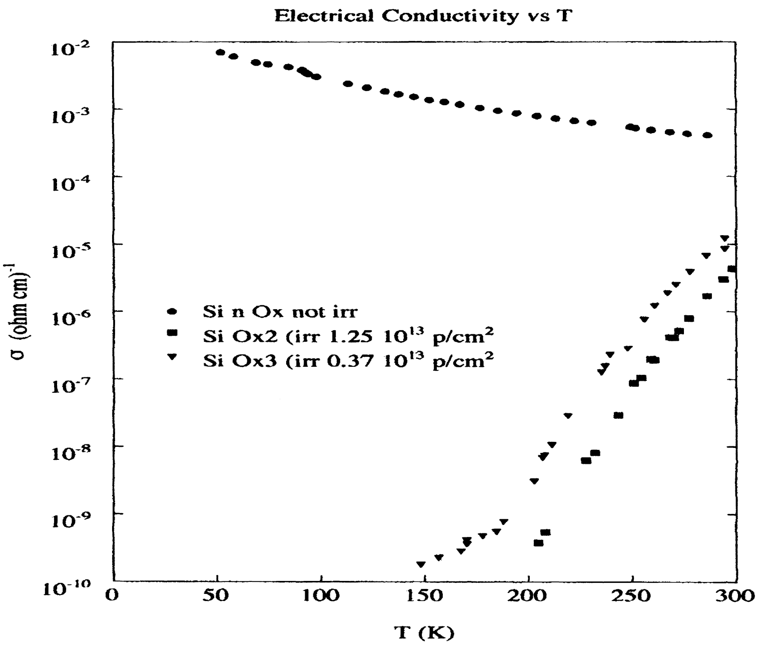

Fig. 3.4. Conductivity of un-irradiated and irradiated silicon as a function of fluence. Ref. [8].

3.4 Epitaxial Material

Very promising results were obtained about a year ago for diodes fabricated on moderately high resistivity epitaxial material [11]. These diodes were processed by Canberra on material manufactured by MACOM in the USA. It consists of a 100 µm, n-type, 900 Ω.cm epitaxial layer grown on a Cz substrate. SIMS measurements indicate that oxygen and carbon levels in the epitaxial layer are considerably higher than in FZ material. This is because these impurities out-diffuse from the Cz substrate during growth. The typical behaviour of the effective doping density versus fluence for the MACOM material is shown in Fig. 3.5 .

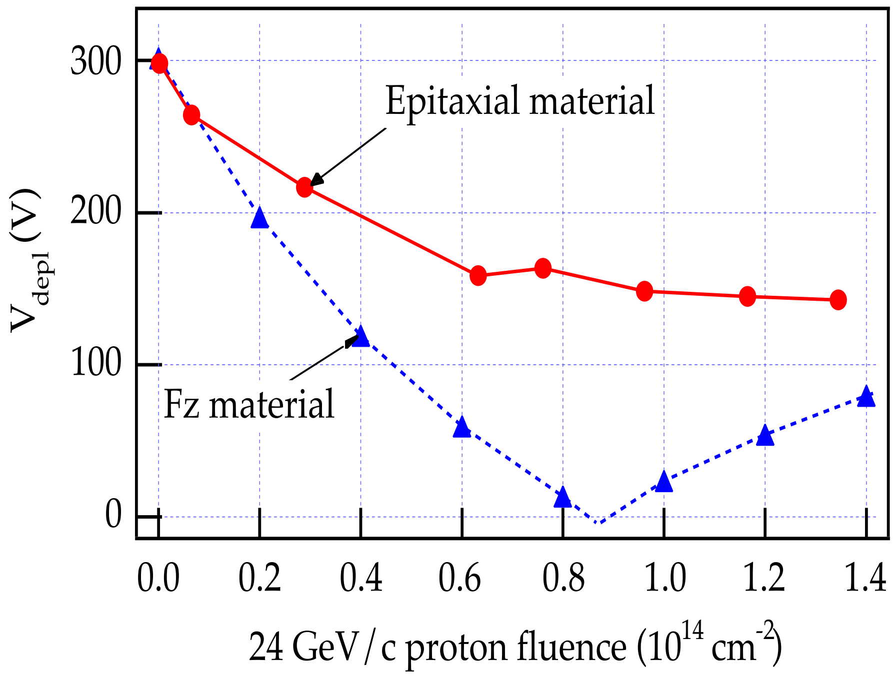

Fig. 3.5. Comparison between evolution of V_{depl} with proton fluence for epitaxial material (results normalised to 300 µm thickness) [11] and Fz material of the same initial resistivity (Fz results are simulated using an established parameterisation for the evolution of N_{eff} with fluence [12]).

It is apparent that doping changes in this material are substantially suppressed. The inversion fluence is found to be a factor two greater than in similar resistivity float zone. The reason for this has yet to be determined as defect characterisation data is still being collected and analyzed. It is likely that the increased oxygen is helping to getter some of the radiation induced vacancies.

Because of this promising result, further material was grown by ITME in Poland. Material of various thicknesses (100, 150 and 200 micron), type, and growth rates (0.5 and 1.0 micron/min) were produced. Growth rates were varied to see if this altered the oxygen and carbon concentrations in the epitaxial layer. These were then processed, distributed and irradiated. A huge amount of data exists and has yet to be fully analysed. Resistivities vary between samples but typically are in the range 1.5 to 6 kΩ.cm, allowing a reasonable depletion voltage. Broadly, the results of measurements on irradiated samples are similar to float zone, i.e. the factor two is not seen for the inversion fluence. On careful examination, the data shows clear differences between samples grown at 0.5 and 1.0 micron/min. SIMS measurements provide important clues to this result. Fig. 3.6 shows SIMS measurements of carbon and oxygen levels in two unprocessed wafers for the two growth rates. The slower growth rate has higher oxygen and carbon concentrations. Clearly there is out-diffusion of oxygen and carbon from the CZ substrate.

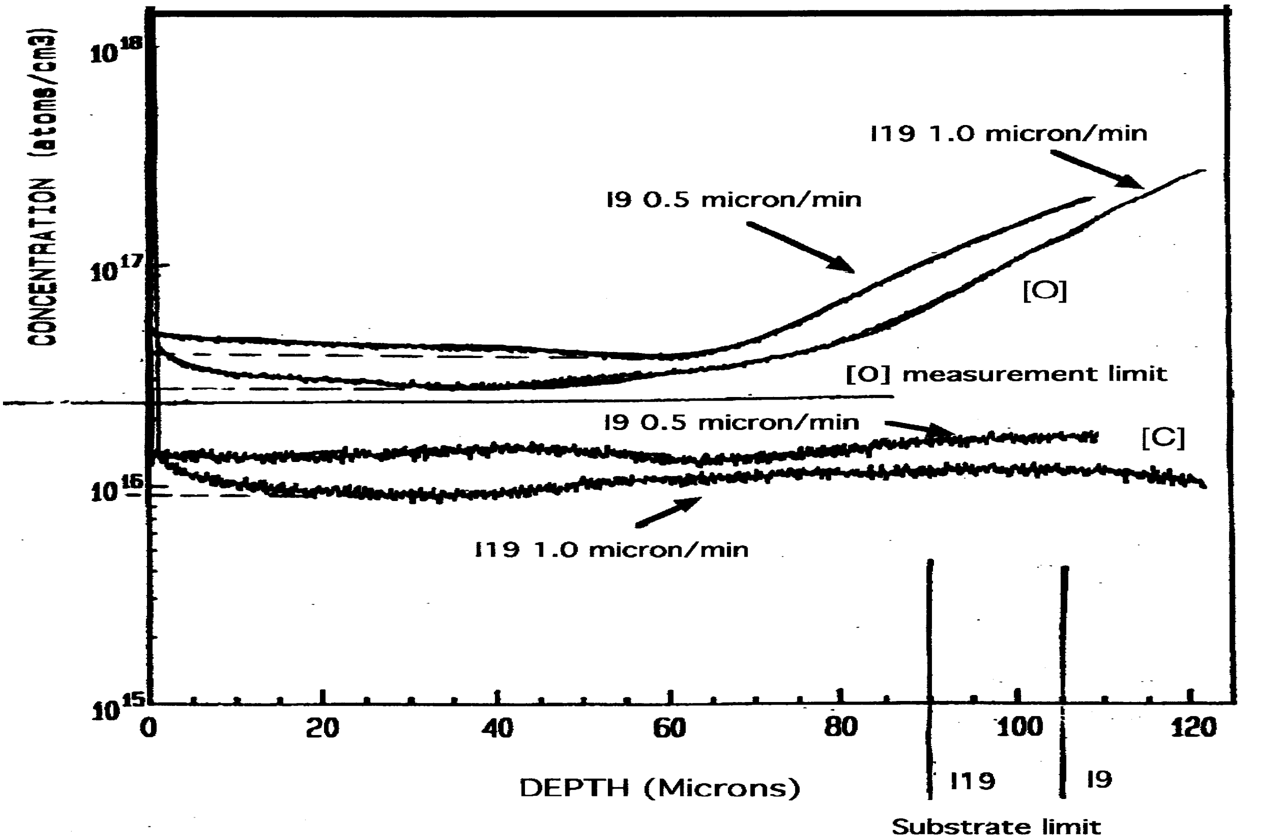

Fig. 3.6 SIMS measurement of oxygen and carbon levels in unprocessed ITME epitaxial material grown at 0.5 and 1.0 micron/min respectively.

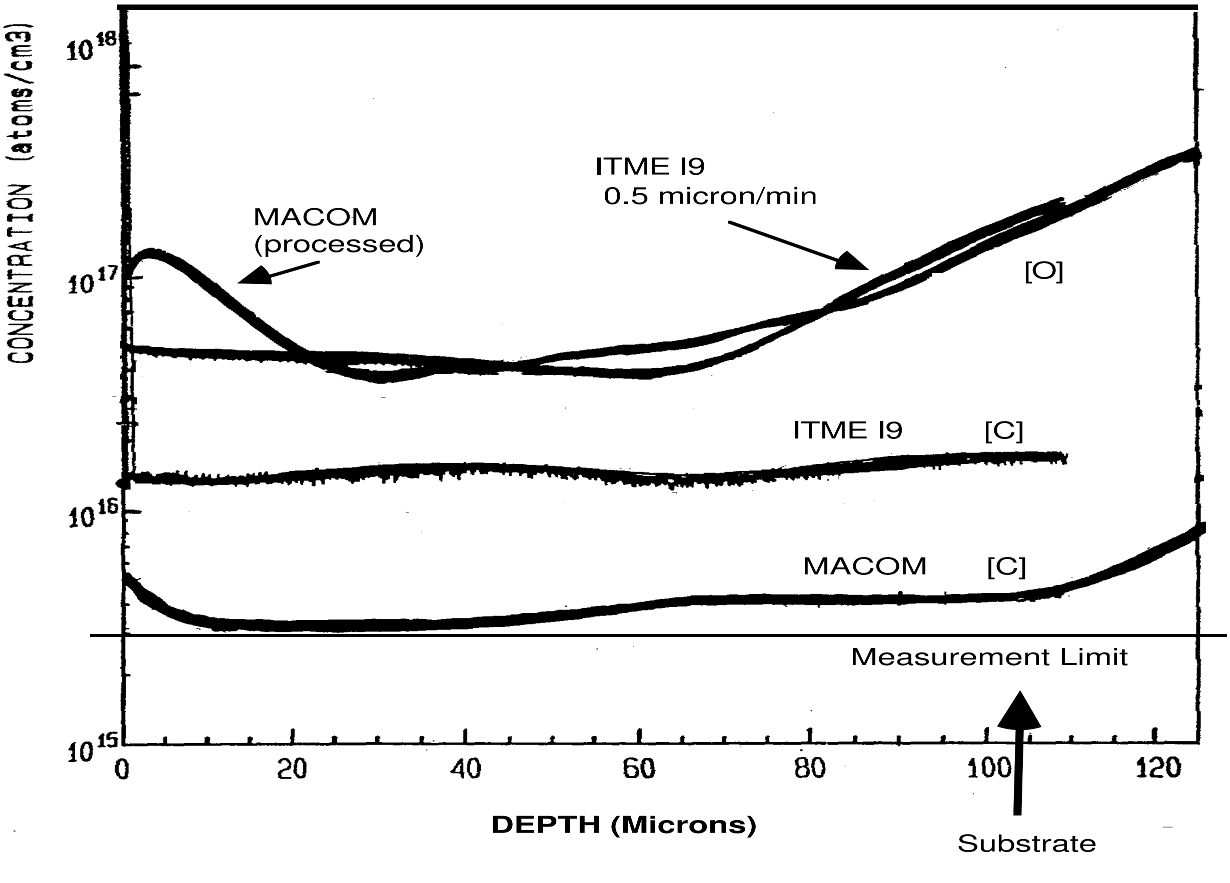

Fig. 3.7 SIMS analysis of a processed MACOM and unprocessed ITME epitaxial wafer.

Fig 3.7 compares the ITME material with the a processed MACOM wafer. The carbon level in the MACOM material is a factor three lower - at/close to the SIMS measurement limit. Diffusion of oxygen from the surface caused by the processing is also apparent. For further comparison, a SIMS measurement for a processed CCD low resistivity p-type Wacker epitaxial wafer is also shown - fig 3.8.

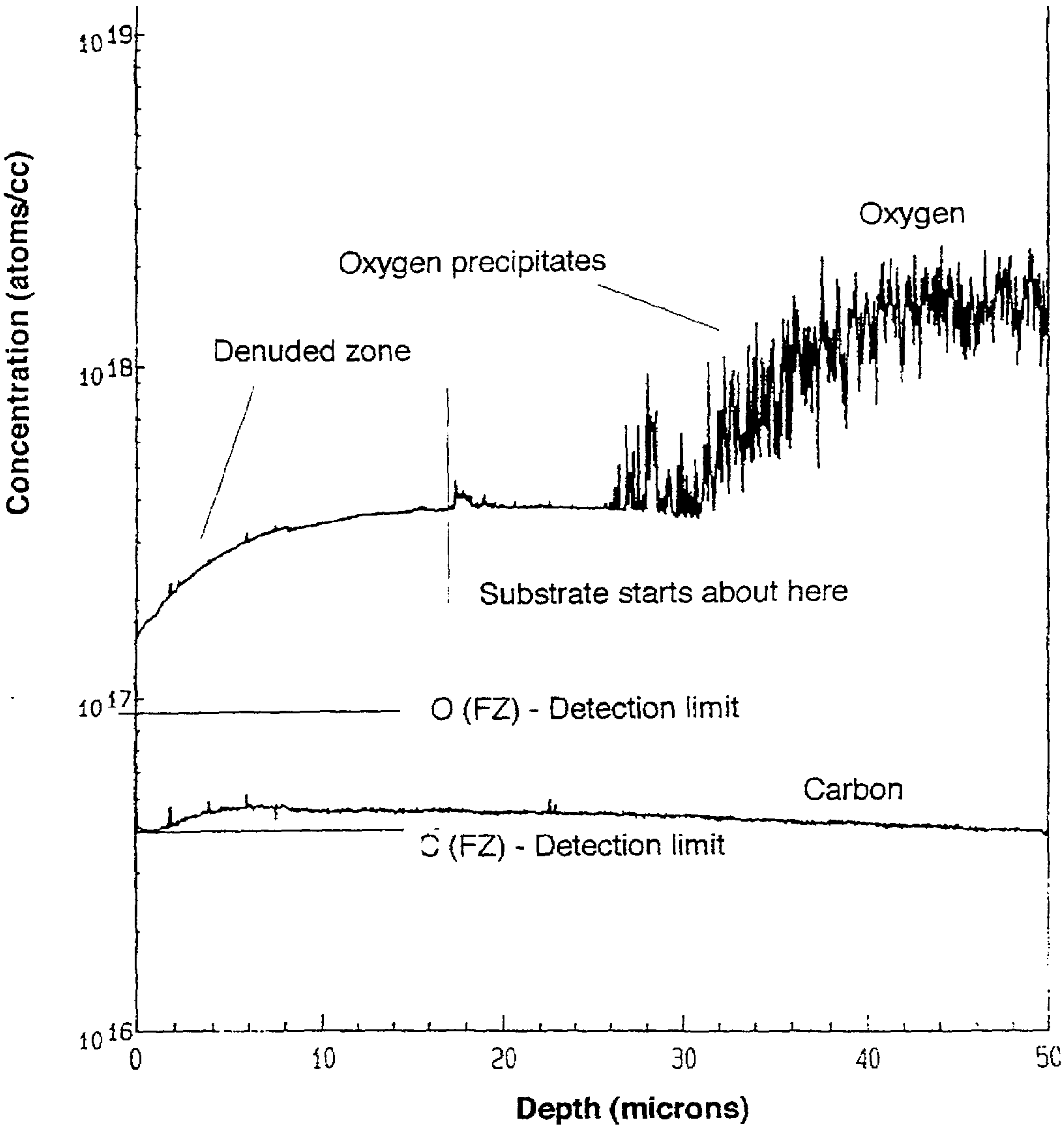

Fig. 3.8 SIMS analysis of a processed EEV CCD wafer. The material is 20 ohm.cm p-type epitaxial supplied by Wacker. The analysis was performed on a CAMECA instrument at Cascade Ltd. UK. This instrument does not have the sensitivity of the one used to obtain the data in figs. 3.6 and 3.7.

Fig 3.9 shows preliminary results for the depletion voltage of diodes made on various ITME epitaxial diodes which were irradiated at the PS by the CERN group.

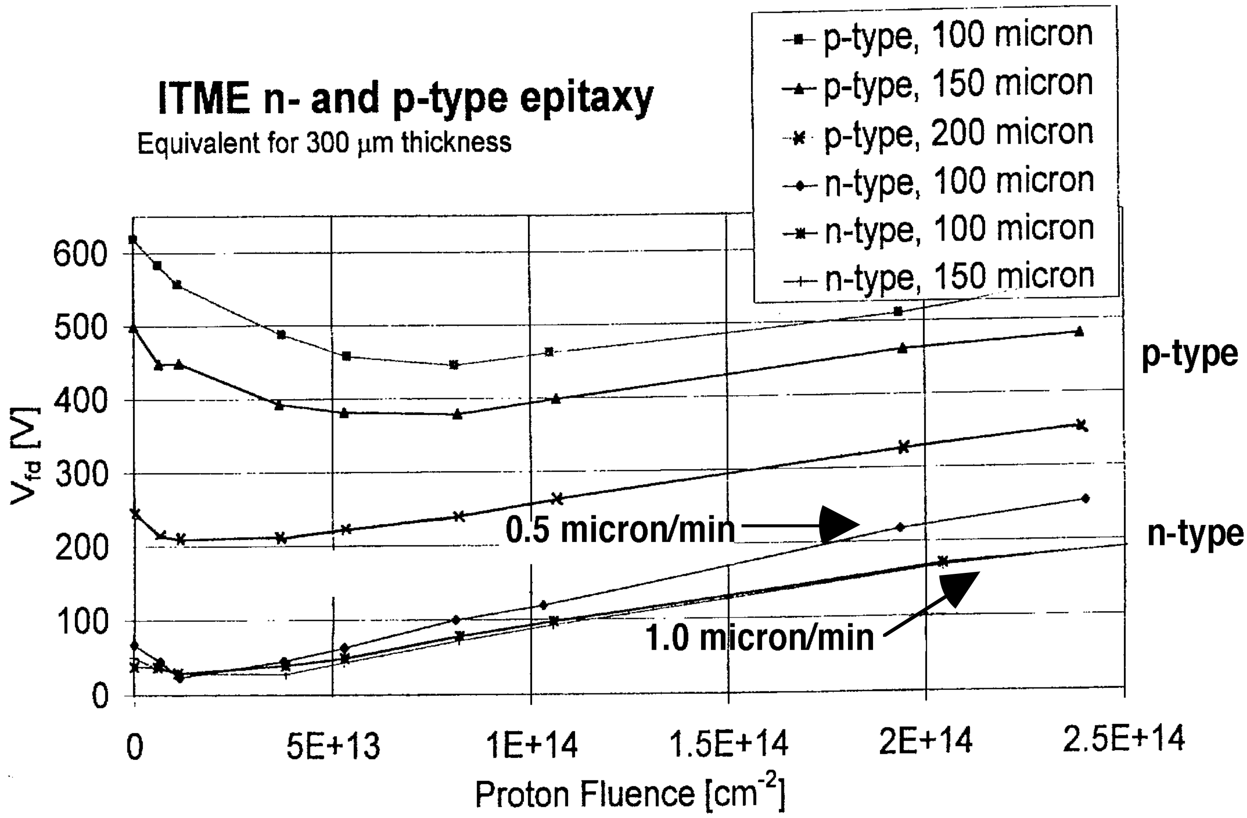

Fig.3.9 First irradiation results for epitaxial diodes manufactured on ITME material. Results for the p-type and n-type diodes are shown. Measured at the PS by the CERN group.

Important features of this data are,

a) The "acceptor" introduction rate (slope of V_{fd} for fluences greater than 10^{14} cm^{-2}) is larger for the 0.5 micron material - a factor 1.4 greater. The leakage current damage parameter is also slightly higher, but better statistics is needed.

b) The depletion voltage for the p-type diodes decreases first and then after around 10^{14} p cm^{-2} increases with a similar slope to the n-type material. There are few results for p-type FZ with which to make a comparison. A comparison with results from the RD2 collaboration, ref. [13], is in progress.

On the basis of this data it would appear that increased carbon levels are not to be recommended. However, it should also be noted that the leakage current parameter is a factor two smaller in CCDs manufactured on Wacker epitaxial. Both carbon and oxygen levels in these devices are higher than in the diodes tested. Only through detailed defect characterisation work can the reason for these differences be understood. In addition, CCDs undergo long and high temperature processes during manufacture associated with intrinsic gettering. This undoubtedly increases the oxygen concentration in the epitaxial layer. The diodes processed on the ITME and MACOM material have received very little high temperature processing. This is an issue that needs to be pursued.

Epitaxial material looks a very promising material for pixel layers at the LHC since these detectors do not require a 300 µm layer for good signal-to-noise performance.

3.5 Oxygenated and Nitrogenated float zone by gas doping.

Oxygenated float zone manufactured using gas doping (OFZ/G) can achieve a maximum oxygen concentration of around 10^{16} cm^{-3}. No significant differences are found between this material and standard float zone - see G. Casse, ref. [2]. However, a different process developed by Wacker using a quartz ring on the float-zone (OFZ/Q) can achieve high oxygen concentrations - fig. 3.10. An order has been placed to manufacture some of this material. From work on epitaxial wafers, we expect OFZ/Q material to be a factor two better than standard float zone.

Nitrogenated float zone manufactured using gas doping (NFZ/G) has been produced but degrades in a similar way to standard float zone - CERN group. Work is in progress to confirm the nitrogen levels in the material. From a negative result using SIMS, the nitrogen concentration is known to be below 10^{15} cm^{-3}. It is thought that higher concentrations are not possible due to the solubility limit.

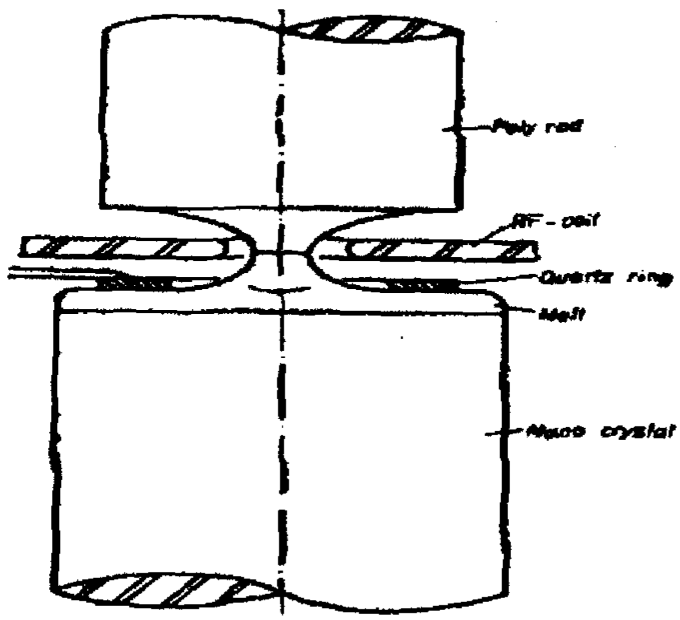

Fig. 3.10 Principle of FZ oxygen doping using a quartz ring - Wacker. Chemitronic GmbH.

4. Defect kinetics and Defect Characterisation

A short summary is given of defect kinetics to provide a framework for understanding the defect characterisation data. Reference [9] should be consulted for detailed information.

A 1 MeV neutron can transfer up to 130 keV to the primary knock-on atom (PKA). An atom with this energy can produce a cascade of many interactions, some of which produce energetic secondary recoils. Each of these terminates in a damage cluster which contains a high density of self-interstitial (I) and vacancy (V) pairs. At the centre of the cluster, where the initial concentration of defects is very high, I-V recombination is the dominant process and most (> 90%) of the primary radiation-induced defects are annihilated in a very short time. Some vacancies combine to form divacancies (V_2) , and possibly larger multi-vacancy complexes - see Section 4.1.

Those interstitials and vacancies which escape initial recombination diffuse through the crystal and react with other defects and impurity atoms, particularly oxygen and carbon. Interstitial oxygen is the dominant sink for vacancies while substitutional carbon is the dominant sink for interstitials. Reaction rates are controlled by the concentrations of defects and impurities and their relative capture radii. Davies et al. [14] have explained optical absorption data after irradiation with 2 MeV electrons by means of a small number of defect reactions. A kinetics model, based on this work but suitably modified, has been used to predict the evolution of defects during neutron irradiation [9]. The list of reactions is shown in Table 4.1. Note that the carbon interstitial, C_i, which is produced by the Watkins displacement reaction $I + C_s \rightarrow C_i + Si$, is mobile and can complex with other impurities.

List A - primary reactions (in the PKA cluster)

I reactions	V reactions	C_i reactions
$I + V \rightarrow Si$	$V + V \rightarrow V_2$	.....

List B - diffusion reactions (outside the cluster)

I reactions	V reactions	C_i reactions
$I + C_s \rightarrow C_i$	$V + V \rightarrow V_2$	$C_i + C_s \rightarrow CC$
	$V + V_2 \rightarrow V_3$	$C_i + O \rightarrow CO$
$I + CC \rightarrow CCI$	$V + O \rightarrow VO$	
$I + CCI \rightarrow CCII$	$V + VO \rightarrow V_2O$	
	$V + P \rightarrow VP$	
$I + CO \rightarrow COI$		
$I + COI \rightarrow COII$		
$I + VO \rightarrow O$		
$I + V_2 \rightarrow V$		
$I + VP \rightarrow P$		

Table 4.1 . Kinetics model reaction scheme [15].

The reactions in list A only have a significant chance of occurring during a PKA cascade. The densities of primary defects in the small volume of the damage cluster are large compared to the concentrations of impurity atoms in the high resistivity material. Consequently the relative introduction rate of divacancies during neutron irradiation is greatly in excess of that during electron irradiation. The reactions in the PKA cluster occur over ~100 ps, whereas the diffusion reactions (list B) take place over a much longer period.

In order to make quantitative calculations, the oxygen, carbon and phosphorus concentrations ([O], [C_s] and [P]) and introduction rates of I, V and V_2 are required. It is now well established that [O] and [C_s] in detector material are typically a few$\times 10^{15}$ cm^{-3}. Electrical measurements yield [P] $\cong 10^{12}$ cm^{-3}. Introduction rates of I, V and V_2 have been calculated from DLTS measurements. These are of the order of 1 cm^{-1}, although there is some controversy between the groups working in this field as to the exact values.

The effectiveness of vacancy capture at oxygen prevents significant VP (E centre) production in high resistivity material. This process is not, therefore, a major factor in the observed doping changes.

Fig. 4.1 provides a nice overview of the defects produced in standard high resistivity float zone. The temperature scan covers almost the entire band-gap. Electron and hole traps are shown in the top and bottom half of the figure respectively.

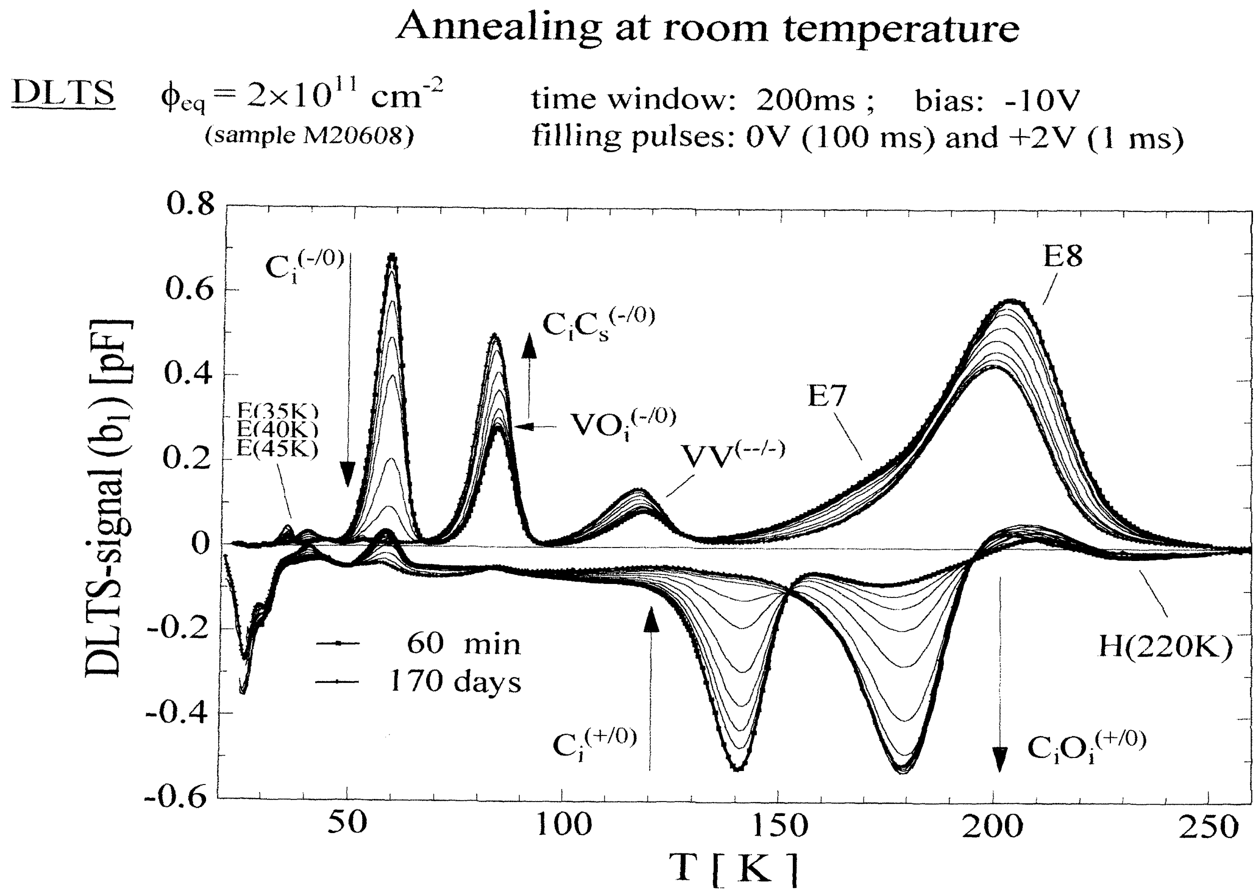

Fig. 4.1 Deep Level Transient Spectroscopy data for an irradiated diode showing annealing behaviour at room temperature. From M. Moll, Hamburg University, ref. [2].

4.1 Observation of new intrinsic defects

The E8 peak is found to anneal at room temperature. Detailed isochronal anneal measurements [16] have shown that it consists of at least two new intrinsic defects - probably multivacancy. They are acceptors with a similar energy level to the singly negatively charged divacancy. These anneal at about 70 and 170 ^{o}C which is why they are denoted E70 and E170 respectively in ref. [16]. In lower resistivity material these levels would be hidden by the vacancy-phosphorus DLTS signal. The annealing of each of these centres is correlated with a large reduction in detector leakage current, [16]. Both defects are too far from mid-gap to explain the magnitude of the changes in the current unless inter-centre charge transfer is occurring - see Section 4.2. The annealing behaviour of defect E170 suggests that it is probably the four-vacancy (V_4). This defect has been observed by EPR after MeV ion implantation [17] and is believed to anneal into the five-vacancy (V_5) at around 170˚C. Fig. 4.1 also shows the strong suppression of the V_2 (=/-) signal at 120K. This has been observed by several workers and it is has been suggested that lattice strain in the cluster acts to reduce the signal from this state [18]. This is discussed again in the section on inter-centre charge transfer.

4. 2 Inter-centre charge transfer

It is possible to calculate the leakage current in an irradiated detector from the measured defect concentrations. These calculations provide compelling evidence that the generation lifetime in devices irradiated with heavy particles is considerably shorter than expected on the basis of standard Shockley-Read-Hall theory . This discrepancy can be explained by inter-centre charge transfer between neighbouring divacancies and other defects (E70 and E170) in the terminal clusters, illustrated in fig. 4.2.

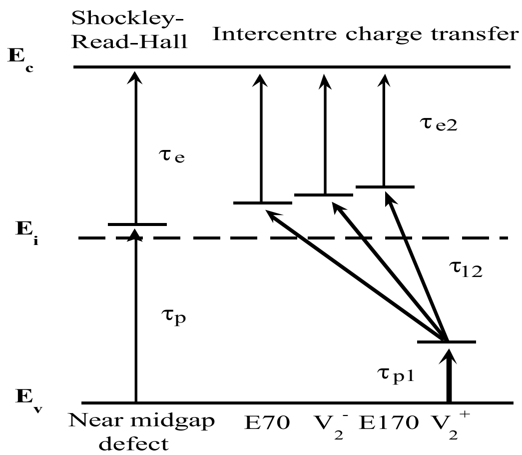

Figure 4.2 Generation processes via Shockley-Read-Hall and Intercentre Charge Transfer (ICT). The latter two step process requires the defects to be in close proximity. From [16].

Simple calculations indicate that the local V_2 density within a typical cluster is ~10^{19} cm^{-3}. Since the extent of the bonding distortion caused by a single divacancy in the lattice is ~10 Å, direct carrier transitions between some of the defects are clearly possible. The divacancy has 4 charge states which give rise to 3 energy levels in the forbidden gap: a donor (+/0) at E_V+0.20 eV; a first acceptor (0/-) at E_C-0.41 eV; and a second acceptor (-/=) at E_C-0.23 eV. By writing general expressions for the rates of emission and capture between any two of these states it is possible to solve for the occupancy of each state as a function of local divacancy density in the cluster - the full calculation is described in [19]. It is found that the occupancy of the first acceptor, denoted f_2, is significantly enhanced over the value predicted by the SRH calculation due to the charge exchange reaction $V_2^0V_2^0 \rightarrow V_2^+V_2^-$. Results are shown in Fig. 4.3.

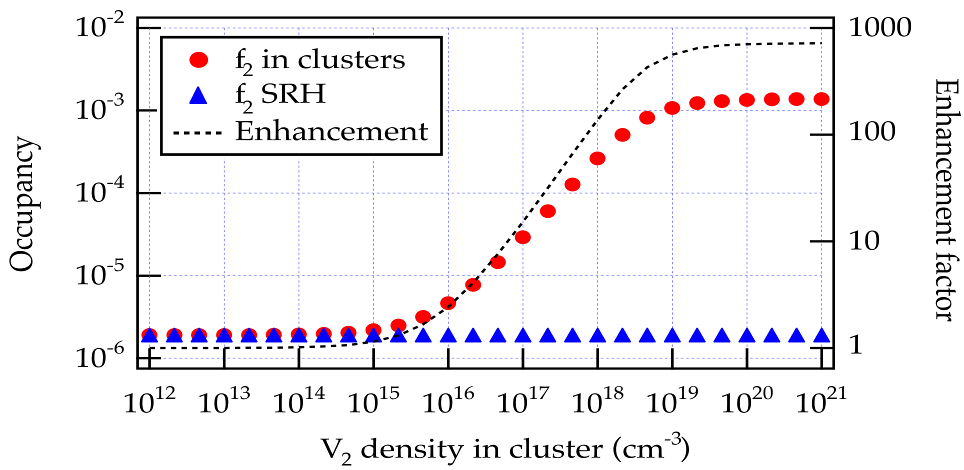

Fig. 4.3 Enhancement of V_2 first acceptor occupancy over SRH prediction due to inter-centre charge transfer [19].

The divacancy, E70 and E170 can therefore make a rather larger contribution to N_{eff} than one would expect. Due to the high emission rates of the states closest to the band edges, inter-centre charge transfer causes a large enhancement in the leakage current. This is discussed further in Section 5.2.

Further evidence that this process is occuring is the suppression of the V_2(=/-) DLTS signal which can be seen clearly in Figure 4.1. Ref. [16] explains how inter-centre charge transfer between the V_2 (-/0), E70, E170 and V_2(=/-) levels can suppress the DLTS signal. Additional confirmation of this idea is shown by the recovery of the signal when the E70 and E170 defects anneal out. The lattice strain explanation and the inter-centre charge transfer idea are probably just alternate ways of viewing the suppression of this signal. An EPR experiment, similar to that performed in ref. [20], would be an important way to confirm that such transitions occur.

4.5. Reverse annealing

Although reverse annealing is an important problem for long-term detector operation, until very recently little progress had been made in understanding its microscopic origins. In the last few months, however, the changes in N_{eff} have been correlated with two experimental observations. The first of these is a growth in the concentration of a bistable acceptor at E_V+0.32 eV [21]. The second is the appearance of the photoluminescence 'W' line [9]. The plot in Fig. 4.4 shows the intensity of this line in 5 samples which were originally irradiated to the same neutron fluence but were then stored at different temperatures for nearly 3 years. The samples have therefore undergone different amounts of reverse annealing. It is clear that the intensity of the line is broadly correlated with the magnitude of the reverse annealing, ΔN_{eff}.

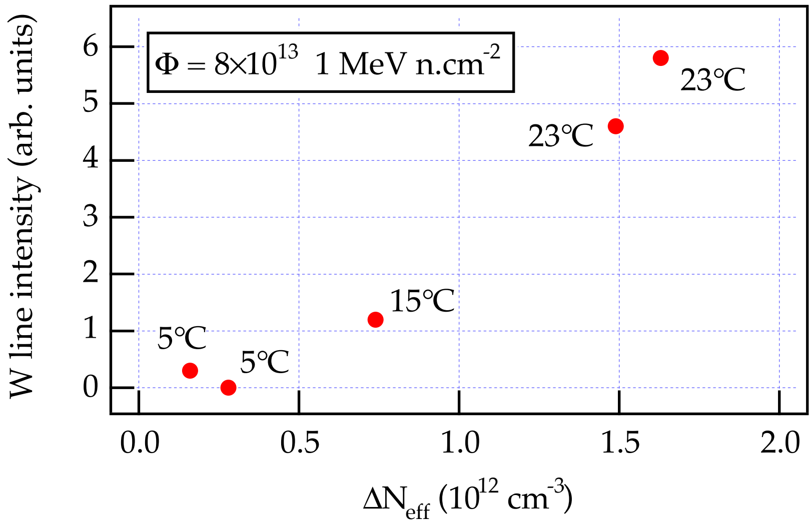

Fig. 4.4. Correlation between strength of the W line and reverse annealing amplitude [9].

The W centre is an intriguing defect. Information may be found in [22]. It does not appear to be associated with any impurity but its production does saturate with increasing dose. It is normally seen after a heavy neutron fluence (~10^{16} cm^{-2}) followed by a 250˚C anneal for 30 minutes. The stress response of the line suggests that interstitials, rather than vacancies, are involved. It therefore seems most likely that the W is an intrinsic centre involving interstitials somehow trapped at a cluster of damage. This new result shows that the W centre can form at room temperature, albeit with a very long time constant.

At present, it is not clear whether the bistable acceptor identified in [21] and the W are the same defect, or, indeed, if they are directly responsible for the changes in N_{eff}. However, some inferences may be drawn. Reverse annealing sets in at ~100˚C during elevated temperature studies [7]. The V_4 anneals into V_5 at a slightly higher temperature (see Section 4.1). Thus, in this temperature region (70 to 170 ºC) defect clusters appear to undergo substantial re-ordering. One can speculate that such a re-ordering might provide a natural mechanism for the creation of the W centre. Defect studies have consistently found that a large number of the interstitials created during irradiation of detector material are 'missing', i.e. unaccounted for by the observed defect complexes (see Section 4.6). It is not, therefore, surprising that the rearrangement of the damage region results in the appearance of an interstitial-related complex.

Recent results with CZ-silicon indicate that reverse annealing is reduced by a factor 1.5 or more. Further measurements are underway.

It is evident that careful studies of the defects produced during reverse annealing, and of the dynamics of cluster re-ordering, are vital if a thorough understanding of the origins of the changes in N_{eff} is to be achieved.

4.6 Summary of defects and introduction rates

Table 4.2 gives the energy level and cross-section for the various defects produced by neutron irradiation. The energy levels are well determined. The cross-section data should be treated with caution. In most cases, DLTS measurements only determine the majority carrier cross-section at a temperature associated with the peak in the spectrum. It is very difficult to get the minority carrier cross-section. The first systematic attempt to get both the electron and hole cross-sections, and their temperature dependence, can be found in reference [23]. Both are needed if estimates are to be made of the contribution of each defect to the macroscopic properties of the material. For consistency, all cross-sections have been taken from one group [24]. The ratio of hole to electron cross-sections have been taken from [23]; if this is not known, then a ratio of one has been assumed.

Defect	Electron or Hole Trap	Energy (eV)	σ_n (cm^2)	σ_p (cm^2)	σ_p/σ_n
C_i	E (- / 0)	-0.11	6.00E-15		1 Note 1
C_iC_s (B)	E (- / 0)	-0.11	3.00E-15		1 Note 1
C_iC_s (A)	E (- / 0)	-0.17	1.00E-15		1 Note 1
C_i	H (0 / +)	+0.28		4.00E-15	1 Note 1
C_iO_i	H (0 / +)	+0.36	1.50E-14	2.00E-15	0.13
VO	E (- / 0)	-0.17	1.00E-14	5.50E-13	56
VP	E (- / 0)	-0.47	3.00E-15		Note 2
V_2	E (= / -)	-0.23	5.00E-15	1.80E-13	36
E170	E	-0.39	1.00E-15		1 Note 1
V_2	E (- / 0)	-0.42	1.00E-15	6.00E-15	6
E70	E	-0.45	1.00E-15		1 Note 1,3
V_2	H (0 / +)	+0.20	5.00E-15	5.00E-16	0.1
EX3	E	-0.52	1.00E-15		1 Note 1
HX1	H	+0.51			

Note 1: Ratio is not measured so one is assumed.
Note 2: This defect is produced at a very low rate in high resistivity n-type silicon. Its parameters are taken from measurements on a low resistivity device.
Note 3: The electron cross section has not been determined. It is assumed that it is similar to the V_2 (-/0).

Table 4.2 Properties of radiation induced defects seen in high resistivity float zone silicon. Energy levels are given relative to the conduction and valance bands for electron and hole traps respectively.

The unknown deep hole trap HX1 has been seen by refs.[25,26]. Ref. [26] contains a detailed investigation of HX1. Ref. [25] contains evidence for EX3. EX3 is probably V_2O. It was observed many years ago in a photo-EPR experiment [27].

Table 4.3 gives introduction rates due to 1 MeV neutron irradiation for the various defects. For consistency, those from ref. [24] have been quoted. The introduction rates for CC and CO are those one would record after all the carbon interstitials have reacted with C_s and O_i. This data can be used to estimate the introduction rates for vacancies and interstitials emerging from the PKA region - or, those that have not recombined or formed into more complicated intrinsic defects, and then go on to react with impurity atoms. These numbers imply introduction rates for the I, V, and V_2, of 1.5, 0.63 and 0.71 cm^{-1} respectively. Ref.

[16] quotes 4.8 cm^{-1} for the divacancy. The discrepancy is being investigated and is mainly due to the choice of a calibration constant by the different groups.

Defect	**Introduction Rate (cm^{-1})**	**Electron Occupancy**	**α (A cm^{-1}) 300K**	**N_{eff}/Fluence (cm^{-1}) 300K**	**ICT factor (Rough estimate)**
C_i (- / 0)	1.50				
C_iC_s (A)	0.38				
C_iO_i	1.19	0.99999			
VO	0.63	2.23E-12	1.01E-21	1.41E-12	
V_2 (= /-)	0.22	1.53E-10	1.18E-21	3.37E-11	
E170	Note 1 0.55	1.04E-06	8.12E-21	5.69E-07	1880
V_2 (- /0)	0.71	6.35E-05	2.01E-19	4.51E-05	24
E70	Note 1 0.40	1.08E-04	6.05E-20	4.33E-05	330
EX3	0.03	0.024	2.81E-18	7.20E-04	
HX1	0.04				

Note 1: Not given in ref. [24]. Inferred from data in ref. [16] which gives the relative introduction rate compared to the V_2 (-/0).

Table 4.3 1 MeV neutron introduction rates for various radiation induced defects

Since the number of interstitials must equal the number of vacancies, one would expect that, $[C_i]/ ([VO] + 2 [V_2])$ should equal one. It is 1.02 and 0.73 for gamma and neutron irradiated diodes respectively. This implies that there are a large number of missing interstitials when terminal clusters are produced. If E170 is the four vacancy, then the ratio of interstitials to vacancies is 0.35. So there are 0.55 to 2.75 cm^{-1} missing interstitials. The number of interstitials relative to vacancies escaping from the PKA region is $[C_i] / [VO]$= 2.38 or an excess of 0.87 cm^{-1} . This is not surprising. The interstitial diffuses faster than the vacancy and many divanacies are formed. Thus, more interstitials than vacancies leave the PKA region. From the discussion in Section 4.5 concerning the W-line it appears that some interstitials are forming into stable complexes.

5. Radiation Damage Models

These describe defect formation and the modelling of irradiated silicon devices.

5. 1. Defect Kinetics

Some discussion of this modelling was given in Section 4. For detailed information see reference [9].

5.2 Device Modelling

To model detectors one must include deep levels in the device equations. To date, only 1D models exist but they do explain the behaviour of irradiated diodes, [10]. Clearly, 2D models are needed. Padova, Imperial College, and Brunel are working on this problem.

A simple model, ref. [28], relating macroscopic parameters with defect concentrations is described in this section to show that the radiation induced changes are now understood reasonably well. One can derive simple relations for the leakage current and effective doping density in the depletion region on the basis of standard Shockley-Read-Hall statistics. The electron and hole emission rates, e_n and e_p, for a defect at energy E_t are given by,

$$e_n = \frac{1}{\tau_n} = \sigma_n v_{nth} N_c \exp\left(\frac{E_t - E_c}{kT}\right) \tag{4}$$

$$e_p = \frac{1}{\tau_p} = \sigma_p v_{pth} N_v \exp\left(\frac{E_v - E_t}{kT}\right) \tag{5}$$

where the various parameters have their usual meaning, see ref. [16]. Thus the electron occupancy of this level, f, in a depletion region is given by,

$$f = \frac{e_p}{e_p + e_n} \tag{6}$$

Using formula (6), can look at the importance of the various levels. This is are shown in figs. 5.1 and 5.2.

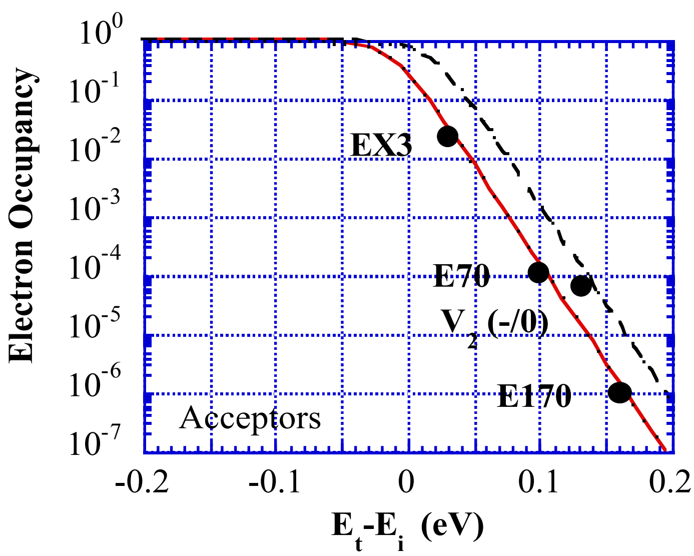

Figure 5.1 Estimated electron occupancy of various radiation induced defects. The solid and dashed lines correspond to σ_p/σ_n of 1 and 10 respectively.

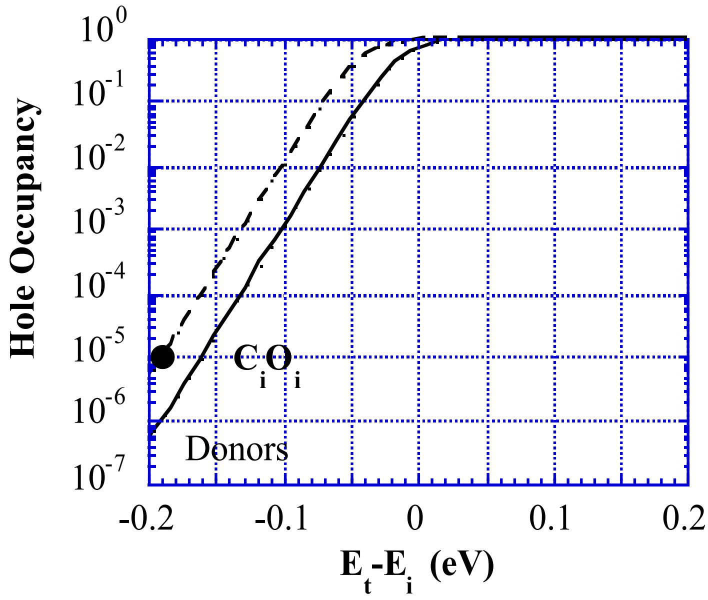

Figure 5.2 Estimated hole occupancy of various radiation induced defects. The solid and dashed lines correspond to σ_n/σ_p of 1 and 10 respectively.

Clearly, there are more levels that can cause the depletion region space-charge to become negative rather than positive, as is seen experimentally. Note that a deep acceptor in the bottom half of the band-gap will always be filled and will contribute maximally to the space-charge but have little effect on the leakage current; for example, the acceptor at E_v + 0.32 eV described in Section 4.5

For simplicity, if one assumes constant defect introduction rates, it is easy to show that the leakage current parameter, α , defined in equation (2) is given by,

$$\alpha = e\sum_{i=1}^{i=N} e_{ni} f_i \beta_i E_i \tag{7}$$

and, the effective doping density, N_{eff} at a particular fluence, ϕ, after inversion, is given by,

$$N_{eff}/\phi = \sum_{i=1}^{i=N} f_i \beta_i E_i \tag{8}$$

β is the introduction rate of the defect, and E is the enhancement factor explained in Section 4.2 for the inter-centre charge exchange process. The subscript i is needed because one must sum over N defect levels.

Table 4.3 also shows the contribution of the various levels to the leakage current and effective doping density. It is difficult to explain the measured leakage current parameter on the basis of this table. Moreover, ref. [16] correlates E70 with 50 % of the leakage current. The only way to explain the measured leakage current is to use the idea of inter-centre charge transfer, discussed in Section 4.2. Ignoring EX3 for simplicity, then measurements, [16], imply that 50%, 38% and 12% of the leakage current is due to the E70, E170 and V_2^- levels respectively. This enables one to make a crude estimate of the enhancement factor for these levels, quoted in Table 4.2. One can then estimate the total value of N_{eff} / ϕ for each of the key levels, indicated in brackets as,

$$5.7\ 10^{-7} * 1880\ \{E170\} + 4.51\ 10^{-5} * 24\ \{V_2^-\} + 4.33\ 10^{-5} * 330\ \{E70\} + 7.2\ 10^{-4}\ \{EX\}$$

$$= (1.07 + 1.08 + 14.2 + 0.72) * 10^{-3} = 17\ 10^{-3}\ \ cm^{-1} \qquad (9)$$

This would fall to about 3 10^{-3} cm^{-1} when the E70 anneals.

The measured value at 20 °C is about 16 10^{-3} cm^{-1} which anneals to about 9 10^{-3} cm^{-1} after 14 days. Although the calculation is not perfect, it is clear that the changes are mostly understood. Further analysis of the data should lead to better agreement.

HX1 has been ignored in this analysis. It is not clear whether it is an acceptor or donor like defect, [26]. It has a very temperature dependent hole cross-section. At 265K $\sigma_p < \sigma_n$, but at room temperature the reverse is true. Measurements imply that it has a very low electron emission rate at room temperature, so it is not a significant source of leakage current. Most DLTS measurements on high resistivity silicon have used n-type material. It is important to look for deep hole traps in p-type material and study their properties.

6. Hardness Factors

Damage projections for the trackers need reliable and consistent Non-Ionising Energy Loss (NIEL) information. A survey of various papers, and comparisons with measurements lead to the conclusion that the following sources should be used. The hardness factor relates the NIEL of a particular particle to that of a 1 MeV neutron which has a displacement damage cross-section of 95 MeVmb.

6.1 Neutrons

For 10^{-10} to 20 MeV neutrons use P. Griffin (SANDIA), data from ENDF/B-VI, ref. [29]. Above 20 MeV neutron data should not be taken from Van Ginneken, ref. [30], but from Konobeyev et al, ref. [31], 117 for 20 MeV - 400 MeV and Huhtinen and Aarnio, ref. [32], for 805 MeV - 9 GeV.

Taking these three sources for the different energy regions, one finds a consistent energy dependence. The Konobeyev data joins consistently to the SANDIA ones at 20 MeV, unlike the Van Ginneken values.

6.2 Protons

Despite Huhtinen's concern about accuracy, his energy dependence is thought to be more reasonable than the Van Ginneken calculation. At high energies the proton damage and neutron damage are roughly only separated by the Coulomb contribution. This difference gets very small at high energies as compared to the nuclear interaction. Hence one would expect the neutron and proton NIEL to be identical at high energies. The Huhtinen calculation shows this behaviour. Moreover, Huhtinen's calculation for pions agrees with data and in particular explains results in the delta resonance region. So to be consistent, if Huhtinen' s pion data is taken, one should also rely on the proton data. Van Ginneken gives results which are almost identical to Huhtinen at low energies, where the Coulomb interaction dominates. At high energies there is a discrepancy of almost a factor of 2. This means for example that the 24 GeV proton source at the PS would have a hardness factor of 0.5 instead of the 0.9 currently assumed at present. This has been proven already in a dedicated experiment, comparing different particle damage using identical detectors and methods of evaluation , ref. [7]. Urgent work is in progress to clarify this issue.

6.3 Pions

Huhtinens publication should be used. It is the only one available which contains the delta and higher resonances. The hardness factors are in good agreement with ROSE Collaboration measurements at the PSI at around 250 MeV.

6.4 High energy NIEL limit neutrons, protons and pions

From the above sources one finds, hardness factors of 0.446, 0.508, 0.379 for neutrons, protons and pions at 9 GeV. In the peak of the delta resonance the pion hardness factor is 0.946. Fig. 6.1 gives an overview of the recommended displacement damage cross sections for neutrons, pions and protons. Tabulations of this data will be available shortly on the ROSE Web page.

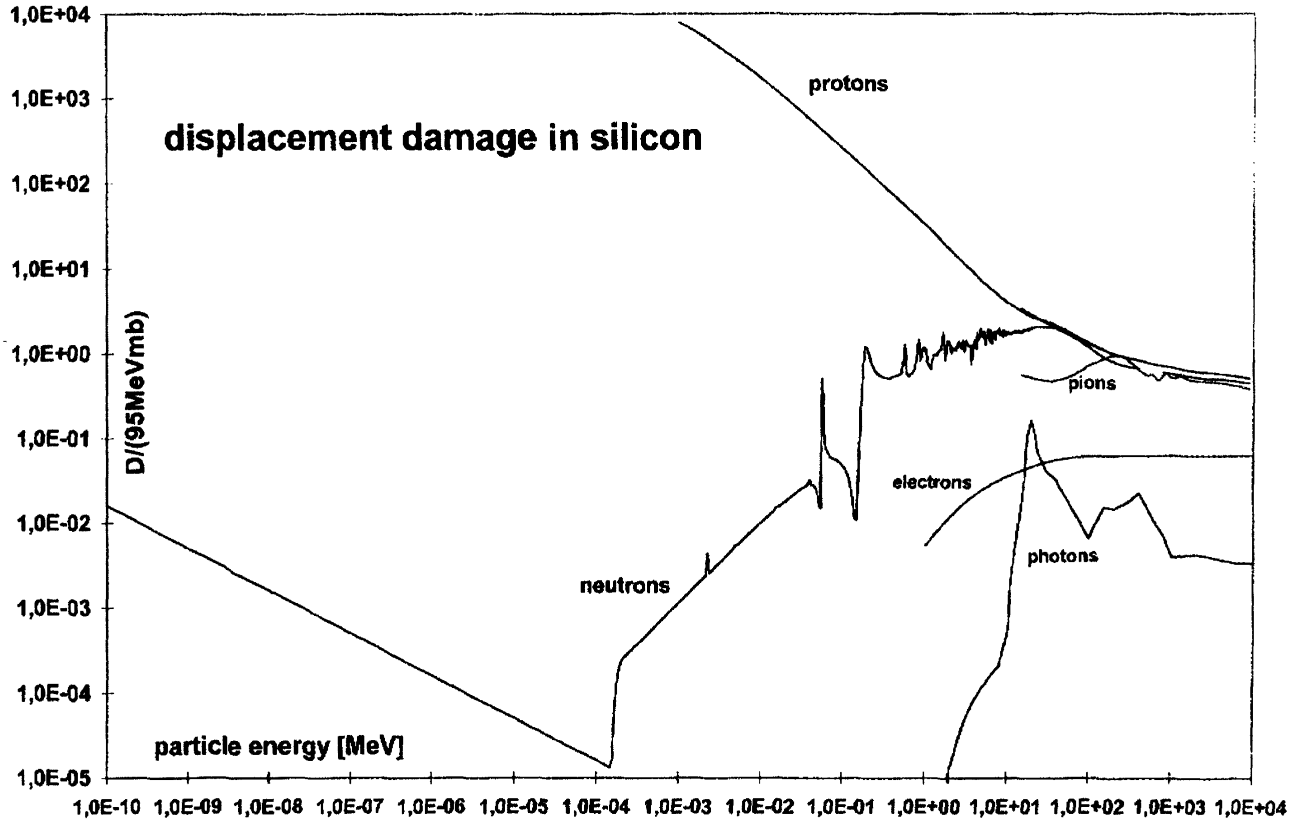

Fig. 6.1 Recommended NIEL data for use in detector damage projections. See text for details.

7. Implications for the LHC detectors.

Clearly the Collaboration has much work still to complete. However, it is possible to provide some guidance to the LHC experiments. This section has been written to stimulate a debate within the community.

- If no new material is forthcoming, two issues need to be addressed:-

a) What resistivity is optimal for operation in the LHC environment?

Multi-Guard structures have been developed that allow higher voltage operation than in the past. Lower resistivity material inverts at a higher fluence. The donor removal rate is much lower than had been thought and this helps to provide positive space charge to combat the radiation induced deep acceptor negative charge.

Fig 7.1 shows a comparsion of two diodes with different resistivities irradiated and measured under identical conditions, ref. [9]. It shows that the lower resistivity material has the advantage for fluences beyond 10^{14} n cm^{-2}. The voltage difference at 2 10^{14} n cm^{-2} corresponds to about 70V.

To answer this question, Fig. 7.2 shows the effect of the revised reverse annealing model and the initial resistivity on the evolution of the depletion voltage during a 10 years operation at LHC. The data hold for the first barrel (R = 30 cm, z = 0) of the ATLAS SCT where at the full LHC luminosity an equivalent 1 MeV neutron fluence of 1.75 10^{13} cm^{-2} is absorbed per year. The calculation is based on the same input and operational scenarios as used in the ATLAS Inner Detector Technical Design Report, Volume II; during the first three years the luminosity is assumed to be at a tenth of its full level, the operational temperature is -7°C, a two days warm-up to 20°C and a 14 days maintenance period at 17°C is foreseen, and numerical values of the damage constants were taken from the corresponding compilation for neutrons given in ref. [33]. As the revised model for the reverse annealing is effectively of first order, the annealing rate does not depend on the absorbed fluence. Reverse annealing is slower at the later stages of the LHC experiment as compared to the original second order model. This gives a reduction in the final depletion voltage of around 50 V for the particular situation discussed here. A major uncertainty in the damage projections results from the error in the fluences and in the damage constants. They are in part due to the difficulty met with the normalization to equivalent 1 MeV neutron values. For purpose of illustration a fluence increased by 50% has been assumed for one of the simulation runs. Finally, two runs with lower resisitivity starting material have been included to demonstrate the improvement in the depletion voltages which could be achieved.

b) The silicon industry trend is to go to lower carbon and oxygen levels. Lower oxygen levels can only make radiation damage effects worse. Material that is ordered in future should not have lower oxygen levels than is measured at present - about 3 10^{15} cm^{-3}.

- Epitaxial silicon with suitable oxygen and carbon levels looks to be a promising choice for the pixel detectors and should give at least a factor 2 improvement. More work, especially on processing effects, needs to be done. If highly oxygenated oxygen float zone (OFZ/Q) can be produced, then this may perform as well. For this reason, we suggest that schedules allow for such material to be used in the inner layers. Outer layers would use material available at present.

● Silicon-tin has the potential to be significantly harder than current material. Results should be available soon.

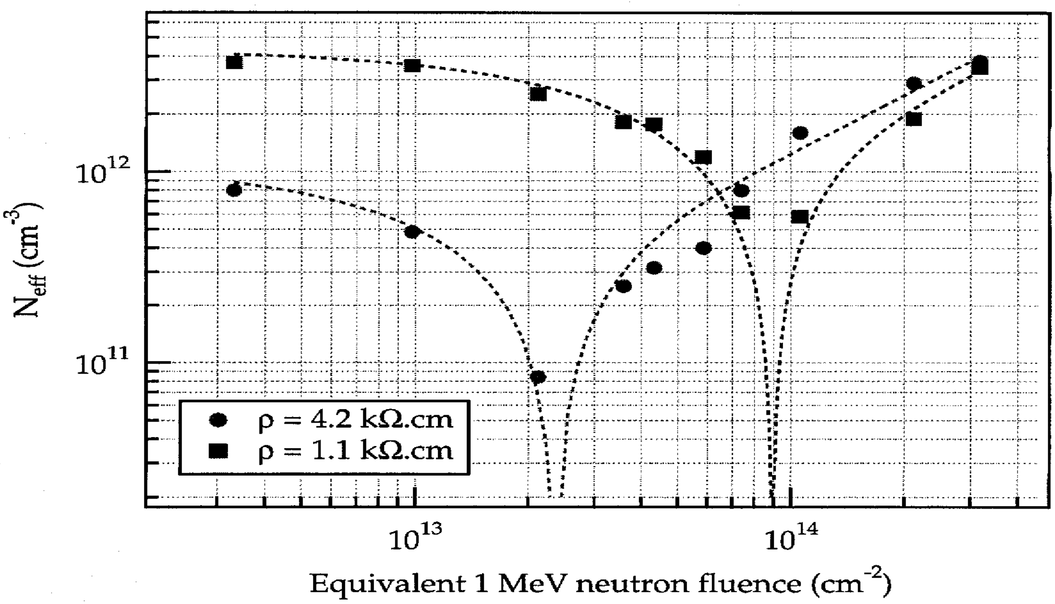

Fig.7.1 Effective doping changes at 20 °c as a function of neutron fluence for high and low resistivity diodes. Measurements were made < 15 days after the end of irradiation. Ref [9].

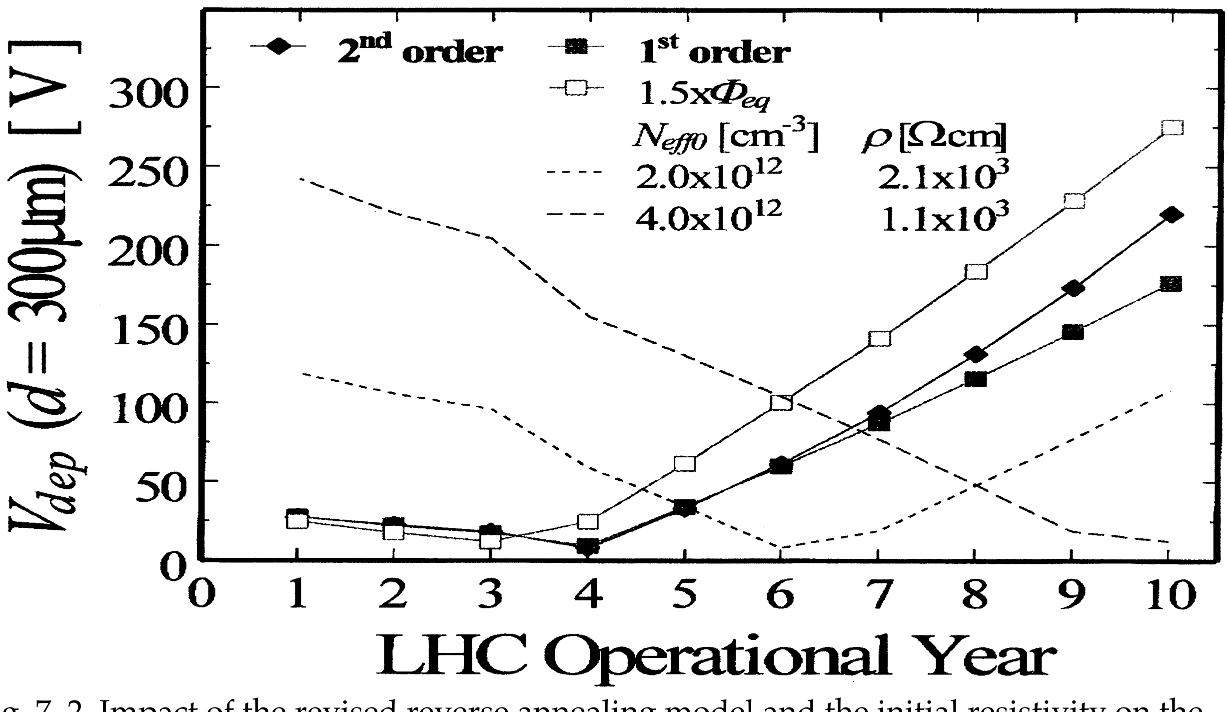

Fig. 7. 2. Impact of the revised reverse annealing model and the initial resistivity on the evolution of the full depletion voltage of a silicon detector at LHC. The fluence, Φ_{eq} = 1.75 10^{13} cm^{-2}, was assumed to be absorbed per year at full luminosity corresponding to the first barrel (R = 30 cm, z = 0) of the ATLAS SCT.

8. Conclusions

This tour of current ideas and recent results demonstrates that our understanding of the underlying physics of radiation-induced bulk damage in silicon has advanced further in the last year. The community now has both the theoretical framework (defect kinetics and device models) and sophisticated characterisation techniques (DLTS, PL, IR, EPR etc.) to understand completely the observed effects. Results on epitaxial material provide the first experimental evidence that defect engineering of radiation tolerant detectors is possible.

It is not fully proven yet, but it seems likely that a high oxygen concentration is beneficial. Epitaxial silicon and probably highly oxygenated float zone (OFZ/Q) can give a factor two improvement in the radiation tolerance. It is also clear that damage clusters contribute to many of the problems, and that their effect is worse due to inter-centre charge transfer. If divacancy production could be suppressed, the material would be extremely radiation hard both from the point of view of the leakage current and the changes in N_{eff}. This requires very high impurity concentrations to ensure that gettering centres are distributed on a similar scale to the PKA cascade. Isoelectronic elements such as germanium (Ge) and tin (Sn) appear to be suitable candidates. However, FZ devices with Ge levels of ~0.1% are known to be no more radiation tolerant than standard detectors. This is probably due to the fact that the Ge-Vacancy complex breaks up below room temperature. Doping with tin is known to suppress V_2 production in CZ material by a factor of ten [34]. Phosphorus at concentrations of around 10^{16} cm^{-3} in the buried channels of CCDs also suppress divacancy production by a similar factor. For this reason, results with silicon-tin are eagerly awaited. Detector manufacturers are concerned about the processing of such material so much development will be required if this material is shown to be radiation hard.

It is also important to note that there are now strong links between the ROSE Collaboration and physicists working on the radiation damage problems of ion-implantation in silicon. These problems represent a technological road-block to achieving very small transistors that will become serious at the beginning of the next century.

9 Outlook and Future plans

This project was scheduled in two phases - ref. [1]. In the first phase, various materials would be tried. In the second phase, the most promising options would be pursued further. The collaboration has almost completed the first phase and will now concentrate on the following areas:-

a) Further development of epitaxial silicon. Issues concerning the processing of this material need addressing.

b) Highly oxygenated float zone (OFZ/Q) will be obtained and evaluated.

c) Silicon-tin will be evaluated for its radiation tolerance. If successful, detector manufacturers will be consulted to identify any technological problems associated with processing such material.

d) Solid-state physics issues that will be pursued include further work on the origins of reverse annealing and the phenomenon of inter-centre charge transfer. It is important to obtain direct experimental evidence for the latter using EPR and other techniques.

References

[1] ROSE Collaboration Proposal, CERN/LHCC 96-23, P62/LHC R&D, (1996)
[2] Transparencies from the 1st and 2nd "Workshop on Radiation Hardening of Silicon Detectors" are available from F. Lemeilleur, CERN.
[3] ROSE Web page - http://www.brunel.ac.uk/depts/phys/rose.html
[4] S. Sotthibandhu, PhD thesis, Imperial College. Rutherford Appleton Laboratory RALT-025 (1994) and references therein.
[5] R. Wunstorf et al., Nucl. Phys. B 23A (1991) 324.
[6] K. Gill et al., Nucl. Instr. and Meth. A **322,** 177 (1992).
[7] H. Feick, PhD thesis, Hamburg University (1997).
[8] M. de Palma, Bari Group, May 1997. ROSE Technical Note in Preparation.
[9] B. C. MacEvoy, PhD thesis, Imperial College. RAL-TH-97-003 (1997).
[10] J. Matheson, M. Robbins, S. J. Watts, CERN RD20/TN/36, Jan. 1995.
[11] B. Dezillie et al., submitted to the International Conference on Radiation Effects on Semiconductor Materials, Detectors and Devices, Florence, Italy, 6-8 March 1996. To be published in Nucl. Instr. and Meth. A. See also CERN/ECP 96-06 (1996).
[12] S. J. Bates et al., CERN/ECP 95-18 (1995).
[13] RD2 Collaboration, Nucl. Phys. B (Proc. Suppl.) **32**, 415 (1993).
[14] G. Davies et al., Semicond. Sci. Technol. **2**, 524 (1987).
[15] B. MacEvoy, S. J. Watts, Invited paper to be presented at GADEST '97, October '97.
[16] S. J. Watts et al., IEEE Trans. Nucl. Sci. NS-**43**, 2587 (1996).
[17] L. Sealy et al., Nucl. Instr. and Meth. B **80/81,** 528 (1993).
[18] B. Svensson et al., Phys. Rev. B 43 no 3, 2292 (1991).
[19] K. Gill et al., accepted for publication in J. Appl. Phys. (1997).
[20] W. Chen et al., Phys. Rev. Lett. 67, 914 (1991).
[21] H. Feick et al., IEEE Nuclear Science Symposium and Medical Imaging Conference, Anahiem, California, November (1996).
[22] G. Davies et al., J. Phys. C: Solid State Phys. **20**, 191 (1987).
[23] A. Hallen et al., J. Appl. Phys. 79(8), 3906 (1996).
[24] M. Moll et al., submitted to the International Conference on Radiation Effects on Semiconductor Materials, Detectors and Devices, Florence, Italy, 6-8 March 1996. To be published in Nucl. Instr. and Meth. A.
[25] E. Fretwurst et al., International Conference on Radiation Effects on Semiconductor Materials, Florence, 1996. To be published in Nucl. Instr. and Meths.
[26] B. Avset, International Conference on Radiation Effects on Semiconductor Materials, Florence, 1996. To be published in Nucl. Instr. and Meths.
[27] Y. H. Lee, T. D. Bilash, J. W. Corbett, Radiat. Eff. **29**, 7 (1976).
[28] S. J. Watts, Invited paper to the 192nd Meeting of the Electrochemical Society, Inc., Paris, 31 August - 5 September 1997.
[29] P. Griffin (SANDIA), data from ENDF/B-VI, unpublished yet but available through private communication to G. Lindstroem, Dec 96.
[30] A. Van Ginneken, Fermilab National Accelerator Laboratory FN-522 (1989).
[31] Konobeyev et al, J. Nucl.Mater. 186 (1992), 117
[32] Huhtinen and Aarnio, NIM A335 (1993) 580.
[33] A. Chilingarov et al., Nucl. Instr. and Meth. A 360 (1995) 432.
[34] B. G. Svensson et al., J. Appl. Phys. **72**, 5616 (1992).

NOTE
Technical Notes are available via the Web Page. This document will be available as a Technical Note by 1 July. A ROSE publications list is also being complied for the page.

APPENDIX 1

2nd WORKSHOP on RADIATION HARDENING of SILICON DETECTORS

CERN, 4-5 February 1997, ECP Conference Room (Building 13-2-005)

Agenda, schedule and list of talks registered (30 January 97)

Tuesday 4 February (building 13-2-005)

9:00 - 10:00 INTRODUCTION

- Turala M.
- Watts S.
- Lindstroem G.
- Lemeilleur F.

10:00 - 12:00 SESSION 1:
Material growth and analysis, Detector processing. (chairman: F.Lemeilleur)

- Sopko B.	Production of FZ silicon wafers and detectors in Prague, 20'
- Nossarzewska E.	Thick, high resistivity silicon epitaxial layers on oxygen rich CZ substrate by ITME, 20'
- Dezillie B.	SIMS, IR and conductance measurements, 15'
- Bruzzi M.	Hall affect measurements on proton irradiated ROSE samples, 15'
- Burger P.	ROSE detector processing by Canberra, 15'
- Evensen L.	Processing of the CERN 2 devices at SINTEF, 10'

12:00 - 13:00 / 14:00 - 17:30 SESSION 2:
Macroscopic measurements (chairman: G.Lindstroem)

- Solanky M.	Forward characteristics of irradiated diodes: data, modeling, comparison of different materials, 20'
- Dezillie B.	Promising results of epitaxy radiation hardness, 10'
- Casse GL.	Radiation hardness comparison between standard and oxygenated FZ materials, 10'
- Li Z.	Electrical characteristics of us processed detectors and radiation results regarding high resistivity high energy implanted wafers, 20'
- Gabathuler K.	Depletion depth and charge loss versus pion fluence, 15'
- Eremin V.	Detailed characterization of silicon detectors irradiated by high energy protons, 15'

- Chilingarov A. Dependence of depletion voltage and capacitance on temperature and frequency, 15'

- Vrba V. C-V and I-V measurements of pure and oxygen enriched detectors, 10'

- Sicho P. Charge collection and charge spread of p+/n pixel detectors irradiated up to 10e15 particles/cm2, 10'

- Albergo S. Very preliminary results from proton irradiation at the LNS facility, 10'

- Chilingarov A. Charge collection in heavily damage diodes, 10'

- Wunstorf R. Surface effects in silicon detectors, 15'

17:30 - 19:00 SESSION 3:
Microscopic analysis and defects, modelling (chairman: S.Watts)

- Svensson B. Evolution of point defects in ion-implanted silicon 15'

- Fretwurst E. DLTS measurements on unirradiated ROSE samples processed by Canberra and the Hamburg group, 15'

- Verbitskaya E. Proton induced defects annealing behavior evinced in basic parameters of silicon detectors, 15'

- Pintilie L. Optical charging spectroscopy: principle of the method and some results on silicon before and after irradiation, 20'

- Watts S. DLTS results and evidence for inter-center charge exchange, 20'

- Moll M. Investigation of annealing effects in irradiated silicon detectors by Deep Level Spectroscopy methods, 30'

- MacEvoy Barry Future directions in kinetics modeling, 20'

5 February 1997 (Building 13-2-005)

9:00 - 10:00 SESSION 4:
Irradiation facilities, systematic effects (chairman: G.Lindstroem)

- Meyer S. Irradiation facilities at Karlsruhe, 10'

- Vasilescu A. Overview on irradiation facilities and the irradiation environment in the CMS and ATLAS SCT in the framework of the NIEL scaling hypothesis, 20'
- Lindstroem G. Neutron irradiation at Demokritos facilities and first results

10:00 - 12:00 SESSION 5:
Reports from new groups, silicon manufacturers and new ideas. (chairman: S.Watts)

- de Boer W.	Silicon activity in Karlsruhe, 10'
- Watts S.	How to correct for signal losses after 10E14 cm-2, 10'
- Lutz G.	Survival of single sided n-bulk detectors after type inversion: a likely explanation and some experimental results, 15'
- Riedler P.	Investigation of clusters defects by small angle neutron scattering,10'
- Thungstrom G.	Fabrication of an integrated dE/E silicon detector by wafer bonding using cobalt disilicide, 10'
- Jones B.	Irradiated silicon as a relaxation Semiconductor, 15'
- TBA	CSEM experience with detector processing, 10'
- Wilburn C.	Micron Semiconductor progress towards radhard structures, 10'
- Lampert M.O.	Manufacturing of detectors for ATLAS by Eurisys, 10'
- Wegrzecka I.	Silicon detectors processed by ITE/Warsav, 10'
Afternoon	**COLLABORATION MEETING**

APPENDIX 2 Distribution of samples to the ROSE Collaboration

Bari: St, O and epi diodes
Brookhaven: St and O wafers for processing, and diodes
Brunel: St, O and epi diodes
Bucharest: St, O and N diodes irradiated with protons at CERN
Catania: St and O diodes
Demokritos: St and O diodes
Dortmund: St, O and epi diodes, strip detectors and CMOS
Firenze: St and O diodes and strip detectors
FNAL: St, O and epi diodes
Hamburg: St, O, N and epi diodes; Si:Sn 1" wafer for processing; p-type diodes
Imperial College: St and O diodes
Karlsruhe: p-type pad and Mesa strip detectors
Kiev: St and O pieces of raw material irradiated with protons at CERN
Lancaster: St, O, N and epi diodes
Padova: St and O diodes and raw materials
Pisa: St and O and epi diodes and strip detectors
Prague-CTU: St and O diodes
Prague- Acad. Sc.: St, O and epi diodes
PSI: St, O and epi pixel detectors
St Petersburg: St, O, N and epi diodes irradiated with protons at CERN